Langmuir

Article

pubs.acs.org/Langmuir

Antigen Detection via the Rate of Ion Current Rectification Change of the Antibody-Modified Glass Nanopore Membrane

Anna E. P. Schibel and Eric N. Ervin*

Electronic BioSciences, 421 Wakara Way, Suite 203, Salt Lake City, Utah 84108, United States

Supporting Information

ABSTRACT: Ion current rectification (ICR), defined as an increase in ion conduction at a given polarity and a decrease in ion conduction for the same voltage at the opposite polarity, i.e., a deviation from a linear ohmic response, occurs in conical shaped pores due to the voltage dependent solution conductivity within the aperture. The degree to which the ionic current rectifies is a function of the size and surface charge of the nanopore, with smaller and more highly charged pores exhibiting greater degrees of rectification. The ICR phenomenon has previously been exploited for biosensing applications, where the level of ICR for a nanopore functionalized with an analyte-specific binding molecule (e.g., an antibody, biotin, etc.) changes upon binding its target analyte (e.g., an antigen, streptavidin, etc.) due to a resulting change in the size and/or charge of the aperture. While this type of detection measurement is typically qualitative, for the first time, we demonstrate that the rate at which the nanopore ICR response changes is dependent on the concentration of the target analyte introduced. Utilizing a glass nanopore membrane (GNM) internally coated with a monoclonal antibody specific to the cleaved form of synaptosomal-associated protein 25 (cSNAP-25), creating the antibody-modified glass nanopore membrane (AMGNM), we demonstrate a correlation between the rate of ICR change and the concentration of introduced cSNAP-25, over a range of 500 nM−100 μM. The methodology presented here significantly expands the applications of nanopore ICR biosensing measurements and demonstrates that these measurements can be quantitative in nature.

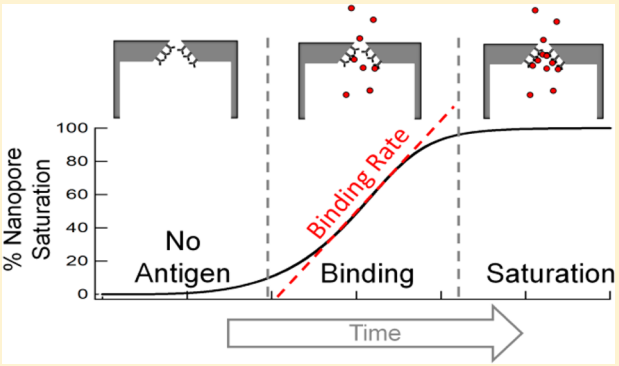

INTRODUCTION

Ion current rectification (ICR) is observed as an asymmetric current−voltage response, defined by a larger current amplitude at one voltage polarity relative to a reduced current amplitude for the same voltage bias at the opposite polarity, and occurs in conical shaped pores due to the voltage dependent solution conductivity within the aperture.[1] This asymmetric current response is influenced by the size of the aperture, the surface charge, and the Debye length (which is inversely proportional to the ionic strength of the electrolyte solution within the aperture).[2−5] A conical pore with a charged surface will exhibit current rectification based on the interaction of the surface charges at the aperture with ions in solution,[1−7] resulting in ion selective transport. For example, in the case of a negatively charged pore, when a positive voltage is applied (relative to the nanopore interior), Na^+ ions will freely migrate from the pore exterior to the interior and Cl^- ions will migrate from the pore interior to the exterior. However, because of electrostatic repulsion between the negatively charged aperture and Cl^- ions, Cl^- transport is hindered, resulting in the accumulation of Cl^- ions within the pore aperture and an increase in conductivity localized at the nanopore aperture relative to the bulk solution. Conversely, when a negative voltage is applied (relative to the nanopore interior), Na^+ ions freely migrate from the pore interior to the exterior while Cl^- ions are electrostatically impeded from entering the pore, resulting in Cl^- ion depletion within the aperture and a decrease in conductivity relative to the bulk solution. In the case of a positively charged pore, the opposite ICR response would occur; Cl^- ions would be free migrate through the aperture while Na^+ ion transport would be hindered, causing Na^+ ions to be depleted within the aperture at positive voltages and accumulated at negative voltages, as the voltage is applied relative to the nanopore interior. The work reported herein describes how to use this ICR phenomenon for concentration dependent analyte detection.

The ICR response of a nanopore can be used to detect a molecule of interest using a strategy referred to here as an ICR biosensing measurement. In this approach, a conical, solid-state nanopore is coated with an analyte-specific binding molecule (e.g., antibodies, biotin, etc.), and the characteristic ICR response of the nanopore is measured before and after analyte molecules (e.g., antigen, streptavidin, etc.) in solution bind to and coat the functionalized aperture,[8,9] with the change in

Received: July 10, 2014
Revised: August 21, 2014
Published: August 26, 2014

response indicating the presence of the analyte of interest. Because this ICR response is surface sensitive, it can be used to detect any analyte of interest that changes the overall size and/or charge of the aperture upon binding and for which there is an analyte-specific binding molecule that can be attached to the internal surface of the nanopore.

In 2005, Siwy et al. first demonstrated that a target analyte could be detected by its influence on the ICR response of a pore functionalized with a molecular-recognition agent.[8] In their studies, a single conical-shaped Au-plated poly(ethylene terephthalate) (PET) nanopore was functionalized with biotin, protein-G, or an antibody specific to ricin, which in turn selectively bound streptavidin, immunoglobulin, or ricin, respectively. The current as a function of voltage response of their functionalized pore was then measured before and after introducing the target analyte. The introduction of the target analyte produced a measurable difference in ICR, and further, only the analyte to which the binding molecule was specific induced an ICR change, indicating that the target had indeed been bound by the nanopore and thus detected. In 2008, Wang et al. presented the ability to characterize the concentration of the drug molecule Hoechst 33258 as it adsorbed to the surface of a conical pore based on the absolute ICR change.[10] In this work a hydrophobic, negatively charged pore contained in a Kapton membrane was exposed to the hydrophobic, cationic drug molecule, Hoechst 33258. As the drug molecule nonspecifically adsorbed to the surface, a difference in ICR was observed, where higher concentrations of the drug molecule yielded larger amplitude differences in ICR. This work demonstrated that the magnitude of the ICR change, i.e., how much the ICR changes before and after antigen binding, could be correlated to the concentration of introduced antigen, although in a highly nonspecific manner. In 2009, Vlassiouk et al. demonstrated ICR-based detection of γ-D-glutamic acid (γDPGA) using conical PET pores chemically functionalized with an antibody specific to γDPGA.[9] Analyte-specific detection via the ICR biosensing measurement has also been reported by Umehara et al., where in 2009 they utilized quartz nanopipettes coated with biotin and IgG antibodies (specific to cancer biomarker proteins interleukin-10 (IL-10) and vascular endothelial growth factor (VEGF)) to detect streptavidin, and IL-10 and VEFG, respectively.[11] In 2010, Ali et al. demonstrated biospecific detection of streptavidin using biotin-functionalized polyimide pores[12] and also reported the ability functionalize the channel with peptide nucleic acid probes to detect the binding of complementary DNA strands.[13] In 2014, Tawari et al. demonstrated concentration dependent detection cytochrome *c* through its specific interaction with a quartz nanopippette coated with human neuroglobin.[14] In all of these studies, the authors demonstrated that a target molecule binding to the aperture of a single nanopore, either specifically or nonspecifically, resulted in a measurable change in ICR. In the present work, we demonstrate the ability to correlate the concentration of the target analyte to the rate at which the ICR changes upon the binding of a target analyte.

Here, a glass nanopore membrane (GNM), which is a single conical-shaped nanopore contained within a thin glass membrane and has been previously thoroughly reported on,[15−21] was coated with a monoclonal antibody specific to the cleaved form of synaptosomal-associated protein 25 (cSNAP-25), in order to generate an antibody-modified GNM (AMGNM). The AMGNM is used to selectively bind its target antigen based on the antigen−antibody binding reaction rather than nonspecific surface interactions, under idealized solution conditions (i.e., in aqueous buffered electrolyte). These AMGNMs were used to detect various concentrations of cSNAP-25, ranging from 500 nM to 100 μM, via the ICR biosensing measurement. In these experiments, the initial ICR of the AMGNM in the absence of the antigen was measured, after which the cSNAP-25 antigen was added to solution and the change in ICR was characterized at regular time intervals, until the rectification level stabilized and 100% AMGNM Saturation was achieved, as depicted in Figure 1.

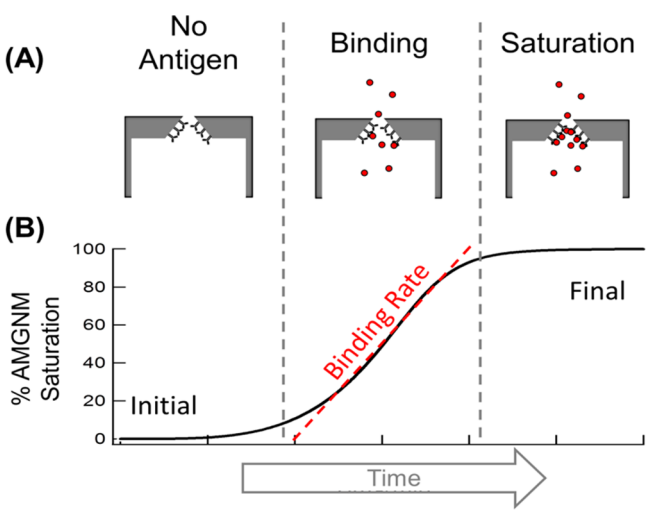

Figure 1. (A) Schematic drawing depicting the binding reaction of a target antigen within the aperture of an antibody modified glass nanopore membrane (AMGNM). (B) Schematic representation of the associated binding curve for the time-dependent attachment of an antigen within the AMGNM aperture.

The detection and quantification of cSNAP-25, which is the cleavage product of botulinum type A (BoNT/A),[22−25] is of particular interest in the field of microbial toxins and neurophysiology due to a growing number of medicinal and cosmetic (e.g., Botox) applications for BoNT/A.[24,26] BoNT/A is one of the most potent toxins known[26] and exists in a dichain state composed of a heavy chain (HC), which is responsible for membrane binding and pore formation, linked via a disulfide bond to a light chain (LC), which is responsible for proteolytic activity.[23−25] In vivo, BoNT/A is internalized into neuronal cells via endocytosis,[18] after which it undergoes a conformational change where the LC is released from the HC into the cytosol where it cleaves its proteolytic target, the SNAP-25 SNARE protein, thus producing cSNAP-25. The cleavage of SNAP-25 prohibits SNARE complex formation at the neural junction,[24−26] thus preventing acetylcholine release/neurotransmission and subsequent muscle contraction. Methods for quantifying cSNAP-25, whether under idealized conditions or in lysed cells, are thus in high demand in order to assess the presence and activity of BoNT.[27,28]

The cSNAP-25 used in these studies is a synthetic peptide comprising amino acids 184−197 of the actual SNAP-25 protein, in addition to a N-terminal cysteine (Cys-Lys-Ala-Asp-Ser-Asn-Lys-Thr-Arg-Ile-Asp-Glu-Ala-Asn-Glu), and exists as a water-soluble ∼1.6 kDa peptide with a net −1 charge at pH ∼ 7 due to four acidic residues (Asp and Glu) relative to three basic residues (Arg and Lys). In order to specifically bind and detect

dx.doi.org/10.1021/la502714b | *Langmuir* 2014, 30, 11248−11256

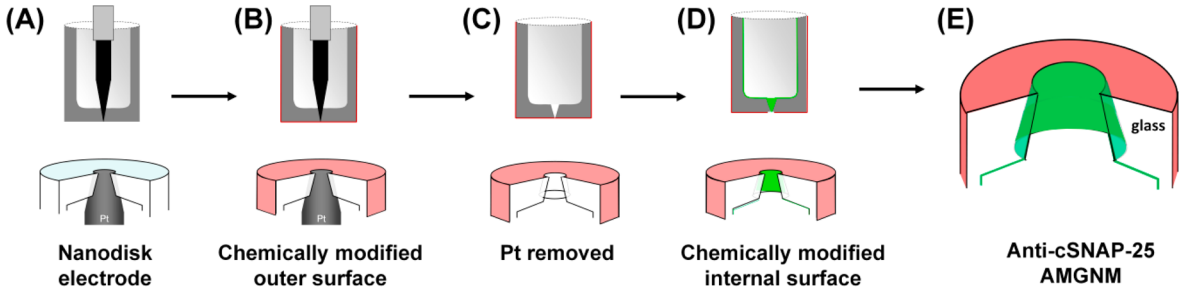

Figure 2. Schematic drawing of the steps associated with fabricating the anti-cSNAP-25 AMGNM, starting from a glass nanodisk electrode. The internal aminosilane coating (3-aminopropyldimethylethoxysilane), heterobifunctional cross-linker (sulfo-SMCC), and antibodies (monoclonal antibody specific to cSNAP-25) are depicted in green, while the nonreactive cyanosilane (3-cyanopropyldimethylchlorosilane) layer is depicted in red.

cSNAP-25, monoclonal antibodies specific to our cSNAP-25 fragment (from a murine host) were used to coat the nanopore aperture, generating the anti-cSNAP-25 AMGNM. Using these anti-cSNAP-25 AMGNMs, we show that cSNAP-25 alters the ICR response of the AMGNM as it binds to the pore aperture and demonstrate for the first time the ability to use a time-dependent ICR biosensing measurement to correlate the antigen detection rate to the antigen concentration.

EXPERIMENTAL SECTION

Chemicals and Materials. NaCl (Sigma), HEPES (Sigma), EDTA (Sigma), $CaCl_2$ (Sigma), NaCN (Sigma), NaOH (Sigma), H_2SO_4 (Acros Organics), 2-mercaptoethylamine-HCl (2-MEA, Thermo Scientific), sulfosuccinimidyl 4-[*N*-maleimidomethyl]-cyclohexane-1-carboxylate (sulfo-SMCC, Thermo Scientific), BupH Phosphate Buffered Saline Packs (Fisher Scientific), 3-cyanopropyldimethylchlorosilane (Gelest), and 3-aminopropyldimethylethoxysilane (Gelest) were used as received. Acetonitrile (Sigma) was stored over a 3 Å molecular sieve. Cleaved SNAP-25 (cSNAP-25, Antibodies-Online) was received as a lyophilized powder, diluted to 1 mg/mL in H_2O, and stored at −20 °C when not in use. Monoclonal antibody (IgG) specific to the cleaved form of SNAP-25 (anti-cSNAP-25, Antibodies-Online) from a murine host was received as a cell supernatant, stored at −20 °C when not in use, and purified (Antibody Clean-up Kit, Pierce) prior to use. Interferent species (used for control experiments) include TCEP (Sigma) and monoclonal antibody specific to BoNT/A LC (R&D Antibodies), which were used as received, and uncleaved SNAP-25 (Creative BioMart), BoNT/A LC (List Laboratories), and BoNT/A (Metabiologics) were filtered via centrifugation prior to use. All aqueous solutions were prepared using H_2O (18 MΩ·cm) from a Barnstead E-pure water purification system.

Antibody-Modified Glass Nanopore Membrane (AMGNM) Fabrication. The complete AMGNM fabrication process, starting with the Pt nanodisk electrode, is depicted in Figure 2. The fabrication of the AMGNM starts in a similar fashion to that of a GNM, which has been previously been described in detail.[15−21] In addition, optical microscopy and AFM images of the GNM can be found in the Zhang et al. reference.[15] Initially, an ∼2 cm length of 25 μm diameter Pt wire (Alfa Aesar) was connected to a tungsten rod (FHC Corp.) using silver conductive paste (Alfa Aesar). The free end of the Pt wire was then electrochemically sharpened to a fine point in 6 M NaCN/0.1 M NaOH using a 3.6 V_{PP} sine wave at 100 Hz from an Agilent 33220A function/arbitrary generator, as described by Melmed et al. and Zhang et al.[15,29,30] This fine point was then further sharpened via a second electrochemical etch in 0.1 M H_2SO_4 using a 15 V (4 kHz) 16 μs pulse waveform and −1.1 V potential, for 1 and 10 s, respectively, as described by Zhang et al. and Libioulle et al.[15,31] The sharpened Pt wire was then inserted into a soda lime glass capillary (0.75 mm i.d. and 1.65 mm o.d., Dagan Corp.), leaving ∼3 mm between the tip and the end of the capillary. Then end of the capillary was then heated using a H_2 flame. As the glass melted, it produced a glass bulb encasing the sharpened Pt wire, which was sealed to a depth of ∼50 μm, as determined via an optical microscope using the diameter of the Pt wire as a visual reference. The bulk of this glass bulb was then manually removed by polishing on 1200 grit sandpaper (Buehler), followed by further polishing down to the sharpened Pt tip using 0.05 μm alumina powder (Buehler) on a polishing cloth (Microcloth from Buehler), in order to create a Pt nanodisk electrode.

Once the Pt nanodisk electrode was created, the outer glass surface surrounding the Pt disk was chemically protected with 3-cyanopropyldimethylchlorosilane to limit nonspecific binding.[16] The nanodisk electrode was cyanosilanized by submerging it in a 2% 3-cyanopropyldimethylchlorosilane solution (in acetonitrile) overnight at room temperature. After the outer glass surface was cyanosilanized, the Pt nanodisk electrode was electrochemically etched to facilitate its removal, in a 1.2 M $CaCl_2$ solution using a 20 V_{PP} sine wave at 100 Hz. This loosened the sealed Pt inside the glass so that it could be mechanically removed, leaving a single conical-shaped nanopore with a larger resistance tip opening relative to a less resistive cone base, contained in a thin glass membrane at the end of a glass capillary, whose outer surface is protected with a cyanosilane. The geometry of the resulting GNM has been extensively characterized; the resulting pore possesses a half-cone angle of ∼12° and a length of 50−75 μM.[15−32] All references to the pore radius refer to the tip opening of the pore.

Antibody attachment to the pore aperture was achieved using standard thiol-based bioconjugate techniques.[33−36] Here, the pore interior was amino-functionalized by filling it with a 2% solution of 3-aminopropyldimethylethoxysilane (in acetonitrile) and letting it sit overnight at room temperature. This aminosilane modification provides free amino sites on the pore aperture that were then reacted under aqueous conditions with the sulfo-SMCC heterobifunctional cross-linker. This cross-linker attaches to the amino groups on the surface silanes via amino-reactive sulfosuccinimidyl ester groups, leaving freely exposed sulfhydryl-reactive maleimide groups for direct antibody attachment via a thioether bond. Sulfhydryl groups were introduced to the monoclonal cSNAP-25 antibody by reducing the disulfide bond in the hinge region of the antibody via 2-MEA under aqueous conditions, after which the reduced antibody was purified using a polyacrylamide desalting column (Thermo Scientific). The solution fractions containing the reduced antibody were identified by measuring the absorbance of each fraction at 280 nm using a UV−vis spectrophotometer (UNICO), resulting in a net antibody concentration of ∼60 μg/mL. The sulfhydryl groups of the reduced antibody were then attached to the free maleimide groups of the cross-linker on the internal surface of the nanopore under aqueous conditions to yield the anti-cSNAP-25 AMGNM. All aqueous reaction steps were performed using 150 mM NaCl, 100 mM sodium phosphate buffer (pH 7.2), and 10 mM EDTA at room temperature. Fully fabricated anti-cSNAP-25 AMGNMs were stored dry at 4 °C.

Ion Current Rectification Measurements. All ICR measurements reported herein were recorded at 20 ± 1 °C, using aqueous buffered electrolyte solutions of 150 mM NaCl, 20 mM HEPES (pH 7.2), and 1 mM EDTA or 150 mM NaCl, 150 mM sodium phosphate buffer (pH 7.2). 150 mM NaCl (Debye length ∼1 nm)[37] was utilized

dx.doi.org/10.1021/la502714b | *Langmuir* 2014, 30, 11248−11256

as it allows for the ICR response of the AMGNM to be characterized and is relevant to biological conditions employed to assess cSNAP-25 concentrations after exposure to BoNT/A.[38,39] Ag/AgCl electrodes were prepared by electroplating a thin layer of AgCl on a 0.25 mm diameter Ag wire. This was done by applying a constant 0.5 mA current between the silver wire (anode) and a Pt wire (cathode) in a 1 M KCl solution until the Ag wire had a visually uniform black-colored coating, i.e., a AgCl coating. The AMGNM was filled with the buffered electrolyte solution, and the internal Ag/AgCl electrode was placed inside the AMGNM capillary. The AMGNM was then inserted into a custom-made polycarbonate experimental cell that contained a second, external Ag/AgCl electrode and was filled with the same buffered electrolyte used inside the AMGNM. Both the exterior and internal AMGNM solutions were exposed to the atmosphere, eliminating pressure differentials across the pore such that potential convection is minimized. ICR measurements were performed using a custom-built high impedance, low noise amplifier and associated instrumentation to apply a voltage sweep across the nanopore, relative to the internal electrode, and record the resulting current response. A voltage of ±1 V was used for all pore functionalization and antigen binding characterization studies, and all current values were measured to two decimal places. In all antigen characterization experiments, the ICR response of the AMGNM was measured prior to introducing antigen to the experimental cell to establish an initial baseline ICR level. After which, the cSNAP-25 antigen was introduced to the experimental cell and ICR measurements were made at 10−60 min intervals, determined from the apparent binding rate, until a stable ICR level was reached. The voltage bias was held at 0 mV between ICR measurements. After use, AMGNMs were rinsed three to six times with experimental buffer and stored dry at 4 °C. The applied voltage, experimental cell temperature, and data acquisition were all controlled via an in-house written LabView program, and data analysis was performed using Igor Pro 6 (WaveMetrics).

RESULTS AND DISCUSSION

AMGNM Functionalization. The degree to which the current is rectified by a given nanopore can be quantified by its rectification ratio (RR_V),[10] which is calculated by dividing the current amplitude at a given positive voltage by the current amplitude at the equal, but opposite voltage ($RR_V = |i_{+V}|/|i_{-V}|$). Prior to any antigen detection studies, the RR_V was used to verify that the chemical functionalization of the AMGNM had progressed as expected during AMGNM fabrication. The current as a function of voltage response of a 180 nm radius negatively charged conical-shaped glass nanopore is shown in Figure 3 (blue trace). This is the response of the bare glass pore, whose outer surface has been modified with the cyanosilane, as described in the Experimental Section, prior to any internal chemical modification. A bare glass surface is composed of negatively charged silicon oxide molecules (pK_a of 1−4),[2,40] which yield a net negative charge to the pore aperture at pH ∼7.[2,41] This net negative charge results in a rectified current response ($RR_V \neq 1$) as a negatively charged aperture will electrostatically attract and preferentially transport positively charged ions (e.g., Na^+) while electrostatically inhibiting the transport of negatively charged ions (e.g., Cl^-). As described above, the associated current through the pore at positive voltage ($i_{+1\ V}$ = 118.78 nA) is increased due to Cl^- accumulation within the aperture relative to the current at the equal negative bias ($i_{-1\ V}$ = −42.87 nA) where Cl^- is depleted within the aperture, yielding a $RR_{1\ V}$ = 2.77. This result is in good agreement with Lan et al., who reported on 30−180 nm radius glass nanopores in 10 mM KCl (pH ∼ 7)[42] that yielded a $RR_{400\ mV}$ of 2−6, respectively. Differences in our measured RR_V value relative to Lan et al. are attributed to differences in electrolyte strength (150 mM NaCl used here relative to 10 mM KCl used by Lan et al.) and different voltages utilized to calculate RR_V (±1 V used here relative to ±400 mV reported by Lan et al.).

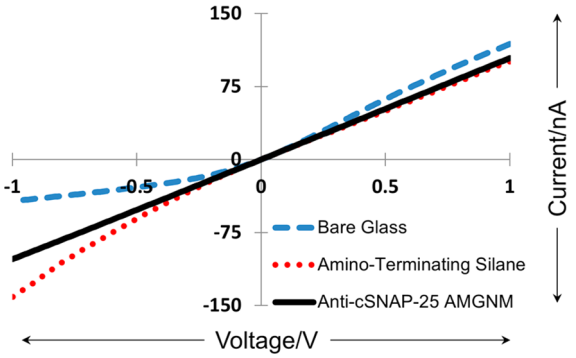

Figure 3. Representative current as a function of voltage traces depicting the ICR response of a 180 nm radius nanopore during the individual surface modification steps associated with fabricating an anti-cSNAP-25 AMGNM. The response of the bare glass nanopore membrane is shown in blue, the response of the nanopore after it is functionalized with an amino-terminating silane is shown in red, and the response of the anti-cSNAP-25 AMGNM is shown in black.

The current as a function of voltage response of a 180 nm radius conical shaped glass nanopore whose internal surface is coated with an aminosilane is shown in Figure 3 (red trace). As described in the Experimental Section, the first internal chemical modification step during AMGNM fabrication is to covalently functionalize the internal surface of the cyano-protected nanopore with an amino-terminating silane, coating the negatively charged silicon oxide groups with positively charged amino groups (pK_a of 9−10)[43] at pH 7, resulting in a positively charged aperture. The now positively charged aperture will preferentially transport Cl^- ions over Na^+ ions. At negative biases, Na^+ accumulates within the aperture and increases the conductance ($i_{-1\ V}$ = −141.36 nA) relative to positive biases where Na^+ is depleted within the aperture and a decrease conductance ($i_{+1\ V}$ = 100.79 nA) is observed, resulting in $RR_{1\ V}$ = 0.71.

Following amino functionalization, the nanopore interior is then reacted with the sulfo-SMCC heterobifunctional cross-linker to introduce free maleimide groups on the glass surface. These maleimide groups are used for antibody attachment in the subsequent modification step, as they react with sulfhydryl groups on the reduced antibody for covalent antibody attachment. Unfortunately, due to the susceptibility of the maleimide group to hydrolysis,[44] the ICR response for this functionalization step is difficult to measure, and thus data for this step are not shown. However, because the exposed maleimides have a pK_a similar to the amino-terminating silane (maleimide pK_a ∼9.5),[45] they are expected to also yield a positively charged pore surface, and thus a Cl^- selective aperture, and the ICR is not anticipated to significantly change between the amino-coated pore and maleimide-coated pore.

The current as a function of voltage response for 180 nm radius anti-cSNAP-25 AMGNM is shown in Figure 3 (black trace). After attachment of the sulfo-SMCC cross-linker to the pore surface, the monoclonal antibody specific to cSNAP-25 is covalently attached to the pore via free sulfhydryl groups on the antibody, as described in the Experimental Section. While the isoelectric point (pI) for this specific antibody has not been characterized, it is expected that as an IgG antibody it will likely have minimal net charge, resulting in a relatively neutral pore

dx.doi.org/10.1021/la502714b | Langmuir 2014, 30, 11248−11256

surface, as most IgG antibodies have a pI of 7.7 ± 1.3.[46,47] The more neutral a surface, the less selective the ion transport, resulting in less ICR and a more ohmic current response, i.e., $RR_V \sim 1$. Here, the current at positive voltage ($i_{+1\ V}$ = 104.26 nA) nearly equals the current at negative voltage ($i_{-1\ V}$ = −102.43 nA), resulting in a $RR_{1\ V}$ = 1.02.

cSNAP-25 Detection via the AMGNM. In order to validate the AMGNM methodology, the response of the anti-cSNAP-25 AMGNM to the presence of cSNAP-25 was characterized. As described above, the AMGNM initially has a relatively neutral surface and yields a nearly ohmic current as a function of voltage response, as shown in Figure 4A (black trace). As the slightly negatively charged cSNAP-25 in solution begins to bind to and coat the internal aperture of the anti-cSNAP-25 AMGNM, the aperture becomes nominally smaller (by 7% at the most, assuming the cSNAP-25 molecule resides is its fully extended form, as estimated from the hydrodynamic radius of each residue)[48] and gains an overall net negative charge, increasing the measured RR_V. The effect of cSNAP-25 binding on the ICR response is shown in Figure 4A by the transition from the black trace (the AMGNM in the absence of cSNAP-25) to the green trace (the AMGNM in the presence of cSNAP-25). Prior to the addition of cSNAP-25, the anti-cSNAP-25 AMGNM has a $RR_{1\ V}$ = 1.02. After the cSNAP-25 is introduced to the experimental cell and the antibody binding of the cSNAP-25 to the surface reaches a steady state, the anti-cSNAP-25 AMGNM has a $RR_{1\ V}$ = 1.35.

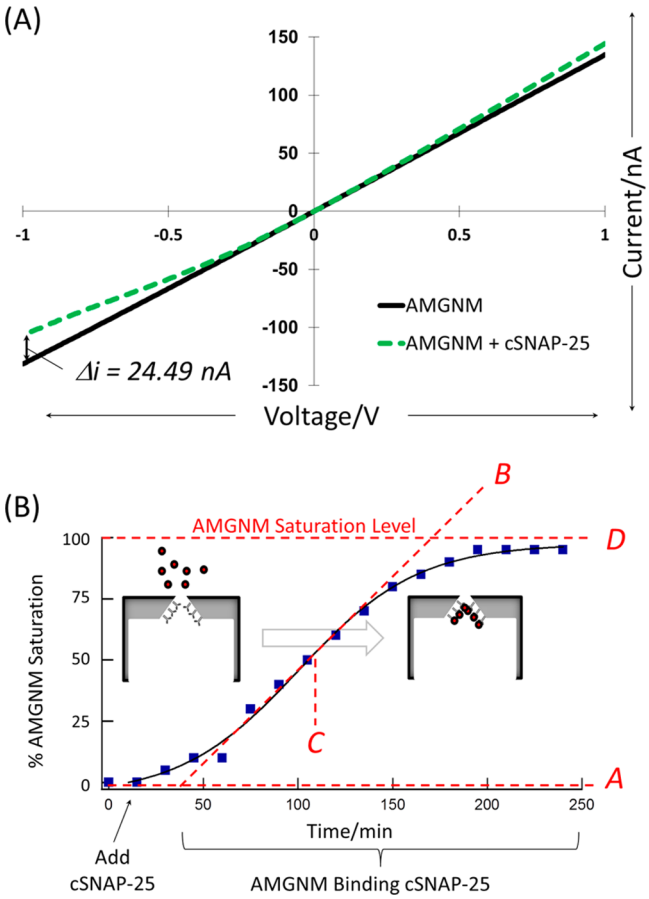

Figure 4. (A) Current as a function of voltage response of a 230 nm radius anti-cSNAP-25 AMGNM before introducing 5 μM cSNAP-25 (black trace) and after binding cSNAP-25 to saturation (green trace). (B) A representative binding curve for the % AMGNM saturation as a function of time for a 75 nm radius AMGNM exposed to 5 μM cSNAP-25. Normalized % AMGNM saturation values were fit to eq 2.

Figure 4B shows the % AMGNM saturation with cSNAP-25 as a function of time for a 75 nm radius anti-cSNAP-25 AMGNM exposed to 5 μM cSNAP-25. The % AMGNM saturation is calculated by the expression

$$\%\ \text{AMGNM saturation} = \frac{RR_V^t - RR_V^{t=0}}{RR_V^{SS} - RR_V^{t=0}} \times 100 \quad (1)$$

where RR_V^t is the RR_V at any given time, $RR_V^{t=0}$ is the initial RR_V measured before cSNAP-25 was introduced to the AMGNM, and RR_V^{SS} is the final steady-state RR_V value reached upon the complete saturation of the AMGNM with cSNAP-25. Among different AMGMNs tested over the course of this work, the change in RR_V, from $RR_V^{t=0}$ to RR_V^{SS}, was found to typically vary anywhere from 0.2 to 0.5. Normalizing the data in this manner allows for the rate of change of the rectification to be compared across different AMGNMs irrespective of the actual rectification ratio values. As is depicted in Figure 4B, the % AMGNM saturation as a function of time plot results in a sigmoidal-shaped curve that can be fit to a five-parameter nonlinear regression model:

$$F(t) = A + \frac{D}{\left(1 + \left(\frac{t}{C}\right)^{(-B)}\right)^E} \quad (2)$$

where A is the minimum asymptote or the initial level of rectification when no antigen is present (i.e., 0%), B is the slope factor or steepness of the curve indicating the rate of cSNAP-25 binding, C is the inflection point of the sigmoidal curve, D is the maximum asymptote or final level of rectification (i.e., 100%), E is the asymmetry factor, and t is time. Both B and C provide information on the kinetics or rate of the AMGNM binding reaction and are thus dependent on the antigen concentration. B is a dimensionless parameter that is directly proportional to the AMGNM binding rate and the concentration of introduced antigen, where larger B values indicate a steeper curve, faster binding, and higher concentration of cSNAP-25. C has the units of time and is inversely proportional to the concentration of the antigen; larger values indicate slower binding and thus lower concentrations of cSNAP-25. Through our experience, B is easier to compare between experiments than C, as it allows for any variations in sample introduction (i.e., the reaction start time) to be excluded from the analysis so samples with different sampling time intervals and sample introduction techniques (i.e., variation in mixing) can be directly related.

The response of the AMGNM was also tested against uncleaved SNAP-25, BoNT/A LC, monoclonal antibody specific to the BoNT/A LC (i.e., antitoxin), whole BoNT/A (HC and LC), and tris(2-carboxyethyl)phosphine (TCEP)—species we anticipate encountering with further development and testing of the AMGNM for botulinum studies. In response to these various potential interferents, the AMGNM maintained a stable baseline (as shown in the Supporting Information file), fluctuating less than ±0.02 from $RR_V^{t=0}$, when the species was introduced to the AMGNM. As described above, the typical ICR change of the anti-cSNAP-25 AMGNM in response to cSNAP-25 ranges from 0.2 to 0.5; thus, the introduction of these "interferent" species yielded at most an ICR change that is less than 10% of the expected AMGNM saturation level response to the cSNAP-25 target antigen. While

dx.doi.org/10.1021/la502714b | Langmuir 2014, 30, 11248−11256

we recognize that more complex solution conditions and interferents may indeed nonspecifically bind to the AMGNM, under the precise conditions utilized here the AMGNM is specific to cSNAP-25.

Concentration-Dependent Characterization. The characterization of 2.5, 5.0, and 10.0 μM cSNAP-25 using the anti-cSNAP-25 AMGNM is shown in Figure 5, along with the

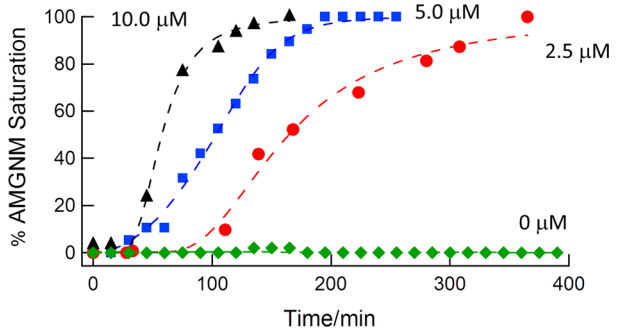

Figure 5. Representative binding curves for the % AMGNM saturation as a function of time for 2.5 μM cSNAP-25 (red circles), 5.0 μM cSNAP-25 (blue squares), and 10 μM cSNAP-25 (black triangles). The 0% AMGNM saturation baseline value (i.e., the response of the AMGNM in the absence of the antigen) is shown for comparison (green diamonds). All four data sets where collected using 50−250 nm radius AMGNMs.

baseline AMGNM response in the absence of antigen (i.e., a blank control). The AMGNM baseline is highly stable, maximum RR_V^t variations of ±0.01 were measured in the absence of target antigen over the course of multiple, 6 h, blank control experiments. Similar to the analysis described above, RR_V^t data for each concentration of cSNAP-25 were normalized, using eq 1, plotted as a function of time, and fit with the five-parameter nonlinear regression model described by eq 2. The rate of cSNAP-25 binding to the AMGNM is concentration dependent, with 10 μM binding proceeding at the fastest rate (i.e., steepest slope and largest B value of the three traces) and 2.5 μM proceeding at the slowest rate (i.e., shallowest slope and smallest B value of the three traces). The steepness coefficient (B) of the best fit for the representative 2.5, 5.0, and 10.0 μM cSNAP-25 data shown in Figure 5 is 3, 7, and 8, respectively.

The steepness coefficient (B) was further determined for other introduced cSNAP-25 concentrations, ranging from 0.5 to 100 μM using the best fit of eq 2 for the respective % AMGNM saturation as a function of time plots. The resulting steepness coefficients (B) are shown as a function of cSNAP-25 concentration in Figure 6. A log−log plot is used here for display purposes, allowing the lower concentrations of cSNAP-25 characterized to be adequately visualized and compared. The dashed line in Figure 6 represents the best fit of the data by a power law model:

$$\log(y) = \log(A) + m\log(x) \tag{3}$$

where y is the steepness coefficient (B), A is the scaling coefficient, x is the concentration of antigen, and m is the slope. A power model is used here to account for the nonlinear trend in the steepness coefficient as a function of cSNAP-25 concentration; i.e., the steepness coefficient exhibits greater concentration dependence at lower concentrations relative to higher concentrations. This behavior is likely a reflection of the dynamic range of the measurement; i.e., higher concentrations

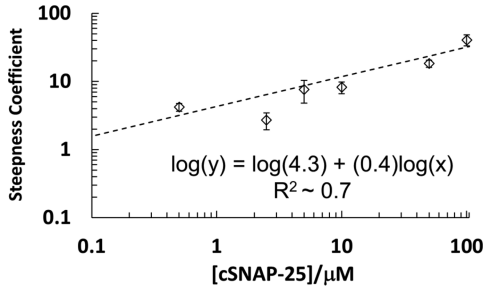

Figure 6. Plot of the steepness coefficient, B, as a function of cSNAP-25 concentration, from 500 nM to 100 μM. These data were fit using eq 3; error bars represent the associated variation in B obtained from a minimum of three trials from individual AMGNMs.

are potentially binding at a rate comparable to the utilized detection interval. The data presented in Figure 6 demonstrate that the rate of RR_V change of the AMGNM is strongly dependent on the concentration of its target antigen, cSNAP-25. From a physical perspective, it is likely that when a high concentration of cSNAP-25 is introduced outside of the AMGNM, it results in a larger flux (via the Brownian motion) of the cSNAP-25 molecules to and through the aperture of the AMGNM relative to lower cSNAP-25 concentrations. This larger flux then results in a higher antigen concentration within the aperture of the AMGNM, followed by more antigen/antibody binding events per unit time, and thus a faster change in the net surface properties of the AMGNM, a faster RR_V change, and steeper binding coefficient (B) relative to lower antigen concentrations.

It should be noted that the applied voltage across the AMGNM is set to zero between individual RR_V measurements and cSNAP-25 is only slightly charged. Electrophoretic migration of cSNAP-25 is therefore unlikely to contribute significantly to the molecular flux to and through the aperture of the AMGNM. Transport into the nanopore, and to the antibody binding sites, should thus be dominated by diffusion. Based on the assumption that the binding process at the AMGNM is diffusion limited and that the AMGNM does indeed reach a state of antigen saturation, the number of antigen molecules required to reach saturation should be similar between experiments, independent from the concentration of introduced antigen. The number of antigen molecules needed to reach saturation can be approximated from the molecular flux and the time required to reach saturation (i.e., the average time it takes from sample introduction to reach the maximum asymptote (see eq 2) or final level of rectification) for a given concentration. The number of cSNAP-25 molecules entering the pore per second can be estimated from the diffusion-based flux (J) into the aperture of the AMGNM:

$$J = 4DrC \tag{4}$$

where J is the flux of the antigen into the aperture, D is the bulk diffusion coefficient of the antigen, r is the radius of the AMGNM aperture, and C is the bulk concentration of the antigen.[49,50] In implementing this equation, we assume that the AMGNM aperture is a perfect sink, i.e., every antigen molecule that reaches the opening aperture enters and stays within the AMGNM, and that there is no antigen diffusion along the outer surface of the AMGNM.[49,50] Here, we calculated the flux of cSNAP-25 for each concentration characterized in Figure 6 by estimating the diffusion coefficient of cSNAP-25 to be 1×10^{-6} cm^2/s,[51−53] and utilizing the intermediate radius size of the

dx.doi.org/10.1021/la502714b | Langmuir 2014, 30, 11248−11256

AMGNMs utilized in this study of 150 nm. The resulting concentration-dependent flux values were then multiplied by the respective time required to reach saturation for each concentration to yield the number of cSNAP-25 molecules required for the AMGNM to reach a saturated state, which is $\sim 2 \times 10^9$ cSNAP-25 molecules, over all concentrations characterized. Complete calculations can be found in the Supporting Information.

From a time-scale-based perspective, the diffusion-limited process limits the AMGNM ICR biosensing measurement to the detection of nanomolar−micromolar analyte concentrations. For example, it takes >6 h to detect 2.5 μM cSNAP-25 (see Figure 5). On the basis of the number molecules needed to reach saturation, one can further estimate how long it would take to reach saturation when examining lower concentrations. For example, dividing the number of cSNAP-25 molecules needed to reach saturation by the flux of molecules entering the pore when characterizing a 1 pM cSNAP-25 sample, it is estimated that it would take $\sim 10^7$ h to reach AMGNM saturation, assuming enough molecules were present to even reach saturation—an unreasonably long time. However, we speculate that the associated analysis time could be decreased by increasing the flux of the target antigen to and through the pore via the use of a driving force (i.e., applied bias and or pressure gradient). These studies, along with studies examining the use of antigen/antibody pairs with differing on/off rates, are currently underway and will be reported on in the future.

Through the course of our work, we have measured a 26% variation in steepness coefficients when using different AMGNMs to detect the same concentration of cSNAP-25 (n = 5). This large deviation is likely due to the relatively large dispersion in AMGNM aperture radii used during this investigation (50−250 nm in radius), and an examination is currently underway to reduce this variation by decreasing the disparity in AMGNM sizes utilized. These results will also be reported on in the future.

AMGNM Reusability. The AMGNM exhibits a stable initial current level, which changes only in response to the presence of cSNAP-25, validating the specificity of the AMGNM ICR biosensing measurement under the experimental conditions tested. Furthermore, the AMGNM can be rinsed free of antigen and reused. Figure 7 shows a continuous trace of the % AMGNM saturation as a function of time for an AMGNM that was utilized to perform two cycles of cSNAP-25 detection. The AMGNM was first exposed to 100 μM cSNAP-25. Once the RR_V had reached steady state conditions, yielding 100% AMGNM saturation, 20 mL of experimental buffer was passed through the 280 μL experimental cell, while applying a constant 500 mV across the AMGNM in an attempt to aid the dissociation of cSNAP-25 from its antibody via convective and electrophoretic forces,[54−56] on the negatively charged bound antigen. As is depicted, this rinsing restored the 0% AMGNM saturation baseline RR_V. Although the dissociation was not explicitly measured over time (represented by the dashed lines in Figure 7), it takes upward of ∼20 min to regenerate the AMGNM baseline with force-assisted antigen dissociation. Once this baseline was restored, 50 μM cSNAP-25 was introduced to the experimental cell and detected. The experimental cell was rinsed again, as described above, again reestablishing the 0% AMGNM saturation baseline RR_V value. We found that an AMGNM could be reused for up to 11 separate detection experiments before the 0% AMGNM saturation baseline RR_V level could no longer be restored through rinsing, or cSNAP-25 exposure would no longer yield an AMGNM response. This appears to be a result of the antibody and/or silane coating detaching from the internal glass surface during the AMGNM cleaning process, as indicated by an observed increase in the RR_V ($RR_{1\,V} > 2$, data not shown) after cleaning, relative to the RR_V of a newly fabricated anti-cSNAP-25 AMGNM ($RR_{1\,V} \sim 1$).

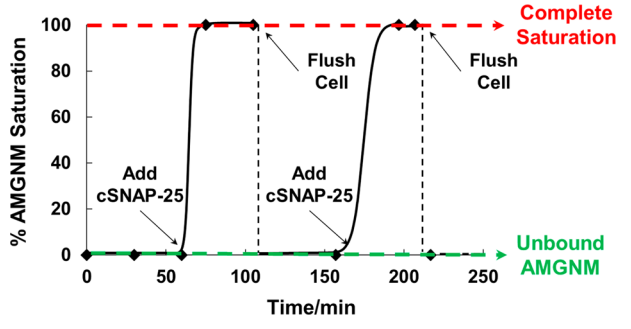

Figure 7. % AMGNM saturation as a function of time for a 50 nm radius anti-cSNAP-25 AMGNM exposed to 100 μM cSNAP-25, then rinsed clean and exposed to 50 μM cSNAP-25, before being rinsed clean again.

CONCLUSION

The results presented here detail the fabrication of antigen-specific AMGNMs and the ability to use the AMGNM to detect the antigen of interest based on the RR_V of the AMGNM. While previous ICR biosensing studies have demonstrated the ability to detect the presence of a target analyte in a qualitative manner,[8−12] we demonstrate that the rate at which the ICR response changes in response to the presence of the target analyte is proportional to the concentration of that analyte through a simple power law model. Specifically, we demonstrate the ability to fabricate AMGNMs coated with the antibody to cSNAP-25 and correlate the rate of ICR change with the concentration of introduced cSNAP-25, over a range of 500 nM to 100 μM, based on a diffusion-limited reaction. Furthermore, we show that the AMGNM can be reused by flushing the antigen off of the aperture, restoring its initial ICR baseline. The methodology presented significantly expands the applications of nanopore ICR biosensing measurements and demonstrates that these measurements can be used quantitatively for antigen-specific detection and potentially as a tool to probe the kinetics of antigen−antibody binding processes.

ASSOCIATED CONTENT

Supporting Information

RR_{1V} as a function of time plots for our interferent species; flux calculations and number of molecules needed to reach saturation of the AMGNM. This material is available free of charge via the Internet at http://pubs.acs.org.

AUTHOR INFORMATION

Corresponding Author

*E-mail ervin@electronicbio.com (E.N.E.).

Notes

The authors declare no competing financial interest.

■ ACKNOWLEDGMENTS

This work was supported by NIH grant 1R43NS074610 and the CBD program W81XWH-11-C-0085. In addition, we thank Dr. Geoffrey Barrall and Melissa Poquette of Electronic BioSciences for their helpful discussions and review of this manuscript.

■ REFERENCES

(1) White, H. S.; Bund, A. Ion current rectification at nanopores in glass membranes. *Langmuir* **2008**, *24*, 2212−2218.
(2) Wei, C.; Bard, A. J.; Feldberg, S. W. Current rectification at quartz nanopipet electrodes. *Anal. Chem.* **1997**, *69*, 4627−4633.
(3) Karnik, R.; Duan, C.; Castelino, K.; Daiguji, H.; Majumdar, A. Rectification of ionic current in a nanofluidic diode. *Nano Lett.* **2007**, *7*, 547−551.
(4) Siwy, Z.; Dobrev, D.; Neumann, R.; Trautmann, C.; Voss, K. Electro-responsive asymmetric nanopores in polyimide with stable ion-current signal. *Appl. Phys. A: Mater. Sci. Process.* **2003**, *76*, 781−785.
(5) Siwy, Z.; Heins, E.; Harrell, C. C.; Kohli, P.; Martin, C. R. Conical-nanotube ion-current rectifiers: the role of surface charge. *J. Am. Chem. Soc.* **2004**, *126*, 10850−10851.
(6) Siwy, Z. S. Ion-current rectification in nanopores and nanotubes with broken symmetry. *Adv. Funct. Mater.* **2006**, *16*, 735−746.
(7) Siwy, Z. S.; Howorka, S. Engineered voltage-responsive nanopores. *Chem. Soc. Rev.* **2010**, *39*, 1115−1132.
(8) Siwy, Z.; Trofin, L.; Kohli, P.; Baker, L. A.; Trautmann, C.; Martin, C. R. Protein biosensors based on biofunctionalized conical gold nanotubes. *J. Am. Chem. Soc.* **2005**, *127*, 5000−5001.
(9) Vlassiouk, I.; Kozel, T. R.; Siwy, Z. S. Biosensing with nanofluidic diodes. *J. Am. Chem. Soc.* **2009**, *131*, 8211−8220.
(10) Wang, J.; Martin, C. R. A new drug-sensing paradigm based on ion-current rectification in a conically shaped nanopore. *Nanomedicine* **2008**, *3*, 13−20.
(11) Umehara, S.; Karhanek, M.; Davis, R. W.; Pourmand, N. Label-free biosensing with functionalized nanopipette probes. *Proc. Natl. Acad. Sci. U. S. A.* **2009**, *106*, 4611−4616.
(12) Ali, M.; Schiedt, B.; Neumann, R.; Ensinger, W. Biosensing with functionalized single asymmetric polymer nanochannels. *Macromol. Biosci.* **2010**, *10*, 28−32.
(13) Ali, M.; Neumann, R.; Ensinger, W. Sequence-specific recognition of DNA oligomer using peptide nucleic acid (PNA)-modified synthetic ion channels: PNA/DNA hybridization in nanoconfined environment. *ACS Nano* **2010**, *4*, 7267−7274.
(14) Tiwari, P. B.; Astudillo, L.; Miksovska, J.; Wang, X.; Li, W.; Darici, Y.; He, J. Quantitative study of protein-protein interactions by quartz nanopipettes. *Nanoscale* **2014**, *6*, 10255−10263.
(15) Zhang, B.; Galusha, J.; Shiozawa, P. G.; Wang, G.; Bergren, A. J.; Jones, R. M.; White, R. J.; Ervin, E. N.; Cauley, C. C.; White, H. S. Bench-top method for fabricating glass-sealed nanodisk electrodes, glass nanopore electrodes, and glass nanopore membranes of controlled size. *Anal. Chem.* **2007**, *79*, 4778−4787.
(16) White, R. J.; Ervin, E. N.; Yang, T.; Chen, X.; Daniel, S.; Cremer, P. S.; White, H. S. Single ion-channel recordings using glass nanopore membranes. *J. Am. Chem. Soc.* **2007**, *129*, 11766−11775.
(17) Lan, W.-J.; White, H. S. Diffusional motion of a particle translocating through a nanopore. *ACS Nano* **2012**, *6*, 1757−1765.
(18) Lan, W.-J.; Holden, D. A.; Zhang, B.; White, H. S. Nanoparticle transport in conical-shaped nanopores. *Anal. Chem.* **2011**, *83*, 3840−3847.
(19) Ervin, E. N.; Kawano, R.; White, R. J.; White, H. S. Simultaneous alternating and direct current readout of protein ion channel blocking events using glass nanopore membranes. *Anal. Chem.* **2008**, *80*, 2069−2076.
(20) Lathrop, D. K.; Ervin, E. N.; Barrall, G. A.; Keehan, M. G.; Kawano, R.; Krupka, M. A.; White, H. S.; Hibbs, A. H. Monitoring the escape of DNA from a nanopore using an alternating current signal. *J. Am. Chem. Soc.* **2010**, *132*, 1878−1885.
(21) Luo, L.; Holden, D. A.; Lan, W.-J.; White, H. S. Tunable negative differential electrolyte resistance in a conical nanopore in glass. *ACS Nano* **2012**, *6*, 6507−6514.
(22) Fischer, A.; Nakai, Y.; Eubanks, L. M.; Clancy, C. M.; Tepp, W. H.; Pellett, S.; Dickerson, T. J.; Johnson, E. A.; Janda, K. D.; Montal, M. Bimodal modulation of the botulinum neurotoxin protein-conducting channel. *Proc. Natl. Acad. Sci. U. S. A.* **2009**, *106*, 1330−1335.
(23) Schmidt, J. J.; Stafford, R. G. Fluorigenic substrates for the protease activities of botulinum neurotoxins, serotypes A, B, and F. *Appl. Environ. Microbiol.* **2003**, *69*, 297−303.
(24) Kukreja, R.; Singh, B. Biologically active novel conformational state of botulinum, the most poisonous poison. *J. Biol. Chem.* **2005**, *280*, 39346−39352.
(25) Baldwin, M. R.; Bradshaw, M.; Johnson, E. A.; Barbieri, J. T. The C-terminus of botulinum neurotoxin type A light chain contributes to solubility, catalysis, and stability. *Protein Expression Purif.* **2004**, *37*, 187−195.
(26) Münchau, A.; Bhatia, K. Regular review: Uses of botulinum toxin injection in medicine today. *Br. Med. J.* **2000**, *320*, 161.
(27) Hallis, B.; James, B. A.; Shone, C. C. Development of novel assays for botulinum type A and B neurotoxins based on their endopeptidase activities. *J. Clin. Microbiol.* **1996**, *34*, 1934.
(28) Fernandez-Salas, E.; Wang, J.; Molina, Y.; Nelson, J. B.; Jacky, B. P. S.; Aoki, K. R. Botulinum neurotoxin serotype a specific cell-based potency assay to replace the mouse bioassay. *PLoS One* **2012**, *7*, e49516.
(29) Melmed, A. J. The art and science and other aspects of making sharp tips. *J. Vac. Sci. Technol., B* **1991**, *9*, 601−608.
(30) Melmed, A.; Carroll, J. An approach to realism in field ion microscopy via zone electropolishing. *J. Vac. Sci. Technol., A* **1984**, *2*, 1388−1389.
(31) Libioulle, L.; Houbion, Y.; Gilles, J. M. Very sharp platinum tips for scanning tunneling microscopy. *Rev. Sci. Instrum.* **1995**, *66*, 97−100.
(32) Zhang, B.; Zhang, Y.; White, H. S. Steady-state voltammetric response of the nanopore electrode. *Anal. Chem.* **2006**, *78*, 477−483.
(33) Cho, I.-H.; Paek, E.-H.; Lee, H.; Choi, J.-W.; Paek, S.-H. Site-directed immobilization of antibody onto solid surfaces for the construction of immunochip. *Biotechnol. Bioprocess Eng.* **2004**, *9*, 112−117.
(34) Bonroy, K.; Frederix, F.; Reekmans, G.; Dewolf, E.; De Palma, R.; Borghs, G.; Declerck, P.; Goddeeris, B. Comparison of random and oriented immobilisation of antibody fragments on mixed self-assembled monolayers. *J. Immunol. Methods* **2006**, *312*, 167−181.
(35) Brogan, K. L.; Wolfe, K. N.; Jones, P. A.; Schoenfisch, M. H. Direct oriented immobilization of F (ab′) antibody fragments on gold. *Anal. Chim. Acta* **2003**, *496*, 73−80.
(36) Predki, P. F. *Functional Protein Microarrays in Drug Discovery*; CRC Press: Boca Raton, FL, 2010.
(37) Heimburg, T. *Thermal Biophysics of Membranes*; John Wiley & Sons: New York, 2008.
(38) Lévêque, C.; Ferracci, G.; Maulet, Y.; Grand-Masson, C.; Blanchard, M.-P.; Seagar, M.; El Far, O. A substrate sensor chip to assay the enzymatic activity of Botulinum neurotoxin A. *Biosens. Bioelectron.* **2013**, *49*, 276−281.
(39) Mizanur, R. M.; Stafford, R. G.; Ahmed, S. A. Cleavage of SNAP25 and its shorter versions by the protease domain of serotype A botulinum neurotoxin. *PLoS One* **2014**, *9*, e95188.
(40) Parks, G. A. The isoelectric points of solid oxides, solid hydroxides, and aqueous hydroxo complex systems. *Chem. Rev.* **1965**, *65*, 177−198.
(41) Sakmann, B.; Neher, E. *Single-Channel Recording*; Springer: New York, 2009.
(42) Lan, W.-J.; Holden, D. A.; White, H. S. Pressure-dependent ion current rectification in conical-shaped glass nanopores. *J. Am. Chem. Soc.* **2011**, *133*, 13300−13303.
(43) Bunimovich, Y. L.; Shin, Y. S.; Yeo, W.-S.; Amori, M.; Kwong, G.; Heath, J. R. Quantitative real-time measurements of DNA

hybridization with alkylated nonoxidized silicon nanowires in electrolyte solution. *J. Am. Chem. Soc.* **2006**, *128*, 16323−16331.
(44) Kalia, J.; Raines, R. T. Catalysis of imido group hydrolysis in a maleimide conjugate. *Bioorg. Med. Chem. Lett.* **2007**, *17*, 6286−6289.
(45) Darnall, K.; Townsend, L. B.; Robins, R. K. The structure of showdomycin, a novel carbon-linked nucleoside antibiotic related to uridine. *Proc. Natl. Acad. Sci. U. S. A.* **1967**, *57*, 548.
(46) Tracy, R. P.; Kyle, R. A.; Young, D. S. Two-dimensional gel electrophoresis as an aid in the analysis of monoclonal gammopathies. *Hum. Pathol.* **1984**, *15*, 122−129.
(47) Li, G.; Stewart, R.; Conlan, B.; Gilbert, A.; Roeth, P.; Nair, H. Purification of human immunoglobulin G: a new approach to plasma fractionation. *Vox Sang.* **2002**, *83*, 332−338.
(48) Chatterjee, S.; Basumallick, I. Thermodynamic studies on amino acid solvation in aqueous urea. *J. Chin. Chem. Soc. (Taipei)* **2007**, *54*, 667.
(49) Berg, H. C.; Purcell, E. M. Physics of chemoreception. *Biophys. J.* **1977**, *20*, 193.
(50) Wang, D.; Gou, S.-Y.; Axelrod, D. Reaction rate enhancement by surface diffusion of adsorbates. *Biophys. J.* **1992**, *43*, 117−137.
(51) Ishimura, M.; Uedaira, H. Natural-abundance oxygen-17 magnetic relaxation in aqueous solutions of apolar amino acids and glycine peptides. *Bull. Chem. Soc. Jpn.* **1990**, *63*, 1−5.
(52) Young, M. E.; Carroad, P. A.; Bell, R. L. Estimation of diffusion coefficients of proteins. *Biotechnol. Bioeng.* **1980**, *22*, 947−955.
(53) Curtis, J. R.; van der Helm-van Mil, A.; Knevel, R.; Huizinga, T. W.; Haney, D. J.; Shen, Y.; Ramanujan, S.; Cavet, G.; Centola, M.; Hesterberg, L. K. Validation of a novel multivariant biomarker test to assess rheumatoid arthritis disease activity. *Arthrit. Care Res.* **2012**, *64*, 1794−1803.
(54) Asanov, A. N.; Wilson, W. W. Oldham, P. B. Regenerable biosensor platform: a total internal reflection fluorescence cell with electrochemical control. *Anal. Chem.* **1998**, *70*, 1156−1163.
(55) Liron, Z.; Tender, L. M.; Golden, J. P.; Ligler, F. S. Voltage-induced inhibition of antigen-antibody binding at conducting optical waveguides. *Biosens. Bioelectron.* **2002**, *17*, 489−494.
(56) Gooding, J. J.; Wasiowych, C.; Barnett, D.; Hibbert, D. B.; Barisci, J. N.; Wallace, G. G. Electrochemical modulation of antigen-antibody binding. *Biosens. Bioelectron.* **2004**, *20*, 260−268.